Spectroellipsometric characterization of Au-Y_2O_3–stabilized ZrO_2 nanocomposite films

George Sirinakis, Rezina Siddique, Kathleen A. Dunn, Harry Efstathiadis, Michael A. Carpenter[a)], and Alain E. Kaloyeros
College of Nanoscale Science and Engineering, The University at Albany-State University of New York, Albany, New York 12203

Lianchao Sun
Angstrom Sun Technologies, Inc., Acton, Massachusetts 01720

(Received 26 April 2005; accepted 15 August 2005)

Nanocomposite thin films consisting of Au nanoparticles embedded in yttria-stabilized zirconia (YSZ) were synthesized at room temperature by radio frequency magnetron co-sputtering from YSZ and Au targets and subsequently annealed in an argon atmosphere. Au microstructure and particle size were characterized as a function of annealing temperature from 600 to 1000 °C by x-ray diffraction, transmission electron microscopy, scanning electron microscopy, and Rutherford backscattering spectroscopy. Spectroscopic ellipsometry was also used to determine the optical constants of the resulting films. In particular, the refractive index of the nanocomposites was found to undergo an anomalous dispersion in the spectral region where the extinction coefficient achieves its maximum. Additionally, the incorporation of Au in the YSZ matrix was found to increase the refractive index in comparison to that of YSZ. At annealing temperatures higher than 800 °C, a good agreement was found between experimental findings and theoretical models using bulk dielectric functions for Au, as modified to account for a reduced mean free path for scattering than that for free electrons. However, for annealing temperatures below 800 °C, an additional offset was required for the optical constants of Au to obtain good agreement between theory and experiment. This behavior was attributed to a relatively high atomic Au concentration in the YSZ matrix.

I. INTRODUCTION

Metal nanoparticles embedded in oxide matrices have been a subject of considerable interest over the past few decades. These nanocomposite systems exhibit unique and customizable optical properties that could be exploited for a plethora of applications, such as high-density information storage devices, ultrafast optical switches, and optical gas sensors.[1–5] However, the successful design of such optical devices requires the ability to customize the optical response of the nanocomposite systems.

In the case of gold (Au), the optical response of Au nanoparticles is dominated by a strong surface plasmon resonance (SPR) band. This resonant behavior is due to the light-induced displacement of conduction electrons with respect to the positive ionic background in the nanoparticle, which results in a restoring force due to surface polarization.[6] This collective, oscillatory motion of the conduction electrons is observed in optical extinction spectra as a selective enhancement of the absorption cross-section of the nanoparticle, with the latter being typically probed by standard absorption measurements. The frequency, width, and intensity of the surface plasmon resonance band depend on the size, concentration, size distribution, and shape of the metal nanoparticle, as well as the dielectric properties of the embedding medium. Therefore, to tailor the optical properties of a nanocomposite film, one needs to ensure precise control over film microstructure and identify a straightforward method for its assessment.

While information regarding the complex refractive index ($N = n + ik$) is important to the technological usefulness of these materials, most of the experimental work to date has focused primarily on studying the extinction coefficient (k). However, knowledge regarding the complex refractive index is crucial for achieving the index-matching necessary for successful integration into

[a)]Address all correspondence to this author.
e-mail: mcarpenter@uamail.albany.edu
DOI: 10.1557/JMR.2005.0411

optical devices. Only a few reports exist on spectroscopic ellipsometry studies of the refractive index (n) of Ag nanoparticles embedded in oxide matrices,[7–10] and even a smaller number for Au.[11] Evidence from these reports indicates that the existence of metal nanoparticles in oxide matrices can drastically alter the overall refractive index of nanocomposite films compared to that of the host matrix. Additionally, the predicted optical properties of nanocomposites, within the context of effective medium theories and size-corrected dielectric functions, are very sensitive to the details of the model used and therefore, previous ellipsometry studies have rarely been found to provide results that are consistent with experimental data, thus further complicating the ability to customize the optical response of nanocomposite systems through systematic design and nanoscale engineering of their structural and compositional properties.

Accordingly, the present work focuses on employing spectroscopic ellipsometry to characterize the optical properties of Au-yttria-stabilized zirconia (YSZ) nanocomposite films synthesized by room-temperature radio frequency (rf) magnetron co-sputtering in combination with post-deposition annealing. To obtain good agreement with the experimental data, the model used for the spectroellipsometric analysis included the gold nanoparticle dielectric function as a fitting parameter within the context of Maxwell–Garnett effective medium theory. Film optical properties were correlated to their microstructure and Au nanoparticle size as a function of annealing temperature.

II. EXPERIMENTAL CONDITIONS

Film depositions were carried out in a custom-designed, stainless steel physical vapor deposition (PVD) reactor equipped with two confocal magnetron sputtering guns, the details of which are given elsewhere.[12] The guns were driven independently by 13.56 MHz rf power supplies. The targets were 5.08 cm in diameter disks of ZrO_2-stabilized with 5 wt% Y_2O_3 (99.9% purity), and Au (99.99% purity). The reactor was evacuated using a combination of a mechanical pump and turbomolecular pump to a base pressure of $\sim 5 \times 10^{-7}$ Torr.

The Au-YSZ films were grown at room temperature on Si(100) substrates. Prior to film deposition, the Si substrates received a standard organic cleaning process consisting of 5-min ultrasonic cleansing first in ethanol and subsequently in acetone baths to remove excess surface organic material. The distances between the substrate and the YSZ and Au targets were set respectively at 50 and 85 mm. Argon (99.999% purity) gas flow rate was set to 5 sccm, and co-sputter deposition was realized at an operating pressure of 5×10^{-3} Torr. Pre-deposition target clean up was performed by sputtering with the shutters closed for 60 min at 200 W rf power for the YSZ target and for 15 min at 20 W rf power for the Au target.

The as-deposited films were subsequently annealed ex situ for 2 h at temperatures of 600, 700, 800, 900, and 1000 °C in 1 atm of argon flowing at a rate of 1 L/min.

III. CHARACTERIZATION TECHNIQUES

Film microstructural and optical properties were investigated by a number of pertinent analytical techniques. Analysis of texture and identification of structural phases of the as-deposited and post-annealed Au-YSZ nanocomposite films were performed using x-ray diffraction (XRD) on a Scintag XDS 2000 x-ray diffractometer. A Cu K_α source was used for x-ray generation. XRD spectra were collected in normal incidence θ–2θ mode with 2θ ranging from 25° to 55° in steps of 0.03°. The collected XRD patterns were compared to the Cu reference patterns from the standard Joint Committee for Powder Diffraction Standards (JCPDS) powder diffraction files—PDF# 802187 for YSZ and PDF# 040784 for Au—for crystalline phase identification.

The average crystallite size D was calculated from the Scherrer formula[13]

$$D = \frac{0.9\lambda}{B \cos \theta} \quad ,$$

where λ is the x-ray wavelength, B is the full width half-maximum (FWHM) of the appropriate elemental XRD peak, and θ is the diffraction angle. XRD elemental peak fit was performed using a Lorentzian curve.[14]

The size and shape of Au nanoparticles were also directly examined by transmission electron microscopy (TEM) in a JEOL 2010F field emission TEM using an accelerating voltage of 200 keV. Cross-sectional specimens were prepared by the focused ion beam liftoff method. Films having thickness of approximately 90 nm were used. Film thickness measurements and plan view imaging were carried out on a LEO 1550 scanning electron microscope (SEM) at a 15-keV primary electron beam energy.

Compositional measurements by Auger electron spectroscopy (AES) yielded a Au content of ~10 at.% measured using a PerkinElmer PHI 600 AES system employing a cylindrical mirror analyzer and a 10 keV primary electron beam. The results of the AES analysis, along with the spatial distribution of Au atoms as function of film depth, were confirmed by Rutherford backscattering spectroscopy (RBS). RBS measurements were performed on a Dynamitron linear accelerator at a primary He^+ ion beam energy of 3.0 MeV.

Spectroscopic ellipsometry (SE) measurements were performed using a variable angle spectroscopic ellipsometer in the wavelength region from 250 to 2000 nm with a step of 2 nm at three different angles of incidence (65°, 70°, and 75°). SE is a non-destructive technique that is intrinsically more sensitive than absorption spectroscopy.

Nanoparticles with radii below 2 nm exhibit a completely damped SPR band, thus making it practically impossible for absorption spectroscopy to obtain accurate information on their microstructure.[6] In contrast, SE can provide such precise information, while allowing the simultaneous determination of the real (refractive index) and imaginary (extinction coefficient) components of the complex refractive index in one single measurement. In this respect, knowledge of the behavior of both parts of the complex refractive index should enable controlled tunability of the optical response of nanocomposite systems through the establishment of systematic microstructure–optical behavior functionality relationships.

In this context, the optical response of the nanocomposite films was modeled using the Maxwell–Garnett[15] (M-G) effective medium theory as applied to a multilayer (air/rough interface/film/SiO_2/substrate) structural model. The free parameters of the model were fitted to the measured ellipsometric data with a linear Levenberg–Marquardt regression algorithm.[16] The dielectric function of the YSZ matrix, which was kept fixed for this work, was determined through the analysis of YSZ films, by a standard Cauchy dispersion with $k = 0$. The dielectric function of Au was modeled by a Drude model for the free electron and four Lorentz peaks to describe the interband transition of Au

$$\epsilon_{Au} = \epsilon_{\text{int erband}} - \frac{\omega_p^2}{\omega^2 + i\gamma\omega} \quad , \tag{1}$$

where ω_p and γ are fitting parameters corresponding to the plasma and the scattering frequency of the free electrons, respectively. For nanoparticles with sizes comparable to or smaller than the bulk mean free path for electronic scattering, the collisions of the free electrons with the surface of the nanoparticle become increasingly important resulting in an effective mean free path smaller than that of the bulk. Accordingly, γ is expected to behave as shown below to account for the additional surface scattering[17]

$$\gamma(R) = \gamma_b + A\,\frac{\upsilon_F}{R} \quad , \tag{2}$$

where γ_b is the scattering frequency of the conduction electrons for bulk Au, υ_F is the Fermi velocity ($\gamma_b = 3.3 \times 10^{13}$ s^{-1}, $\upsilon_F = 1.4 \times 10^{15}$ nm/s for Au),[18] and R is the particle radius as determined through XRD analysis. The coefficient A depends on the details of the scattering processes at the nanoparticle/host matrix interface.[19] As such, A is determined experimentally from the slope in a plot of the full width half-maximum (FWHM) of the SPR band versus inverse particle radius. The FWHM was calculated by doubling the value of the half width at half-maximum (HWHM). The results of this type of analysis for the Au-YSZ system, as reported elsewhere,[12] yielded a value for A of 0.18. This value was therefore used by the present investigators in the model discussed herein to extract the particle size information.

IV. RESULTS AND DISCUSSION

Figure 1 displays RBS data for a set of three different Au-YSZ films annealed at 700, 900, and 1000 °C. The RBS spectrum for an as-deposited Au-YSZ film is also included as baseline. All RBS spectra were plotted as elemental RBS peak intensity versus RBS channel. A comparison of the pre- and post-annealed RBS spectra for all three samples yielded no significant change in the height or FWHM of the Au RBS peak with respect to the Zr peak, indicating that the spatial distribution of Au atoms as a function of film depth is not significantly affected by the thermal treatment, regardless of the annealing temperature used.

Figure 2 displays the XRD patterns for a set of Au-YSZ films annealed at 700, 900, and 1000 °C. The XRD spectrum for an as-deposited Au-YSZ film is also included as baseline. All XRD spectra were plotted as diffraction peak intensity in arbitrary units versus 2θ values (where θ is the diffraction angle) ranging from 25° to 55°. Crystalline phases for tetragonal YSZ and face-centered cubic (fcc) Au were identified for the pre-annealed sample.

As the annealing temperature increased, the peaks became sharper and more intense, indicating a rise in the degree of crystallinity of the YSZ matrix, along with an increase in the average size of the Au crystallites. The average crystallite size for Au was calculated from the Scherrer formula using the (111) reflection for Au,[13] with the results of this analysis being summarized in Table I. Additionally, because the total Au atom concentration and distribution is basically similar for all samples, as indicated by the RBS data, the increase in the average Au nanoparticle size with annealing temperature imply that Au nanoparticles grow by depletion of

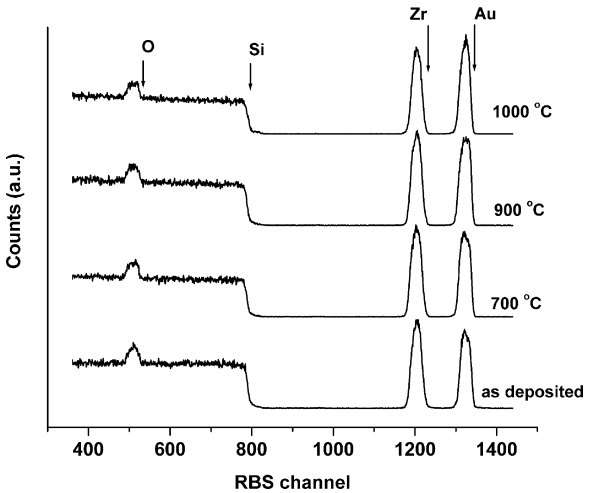

FIG. 1. RBS spectra of Au-YSZ nanocomposite films as a function of annealing temperature.

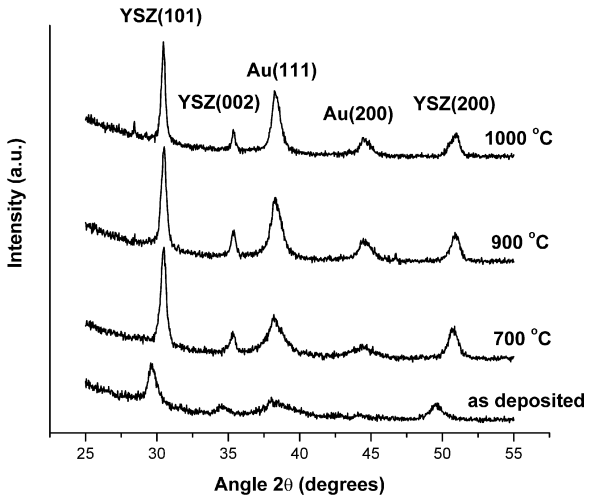

FIG. 2. X-ray diffraction patterns of Au-YSZ nanocomposite films as a function of annealing temperature.

Au atoms from other sites within the surrounding YSZ matrix, most probably through a solid state diffusion mechanism.[20]

Figure 3(a) displays a typical cross-sectional bright field TEM image of the heat-treated Au-YSZ nanocomposite, in this case for a sample annealed at 900 °C. TEM imaging shows the presence of individual Au nanoparticles, and potential aggregates of nanoparticles, that are distributed throughout the YSZ matrix. Higher-magnification TEM yields visible Au lattice planes within individual nanoparticles, as shown in Fig. 3(b). In this context, the edges of single nanoparticles are defined by the contours where the atomic planes change direction or terminate at the interface with the YSZ matrix. High-resolution TEM studies also revealed that the nanoparticles are most likely to exhibit an approximately spherical shape with a mean diameter of 9 nm and a standard deviation of 1.5 nm. These values are consistent with XRD findings.

SEM micrographs of the typical surface topography of Au-YSZ nanocomposite films are shown in Figs. 4(a), 4(b), 4(c), and 4(d) for, respectively, an as-deposited film and films annealed at 700, 900, and 1000 °C. Corresponding histograms of the surface particle size distribution are also shown in Figs. 5(a), 5(b), 5(c), and 5(d). An

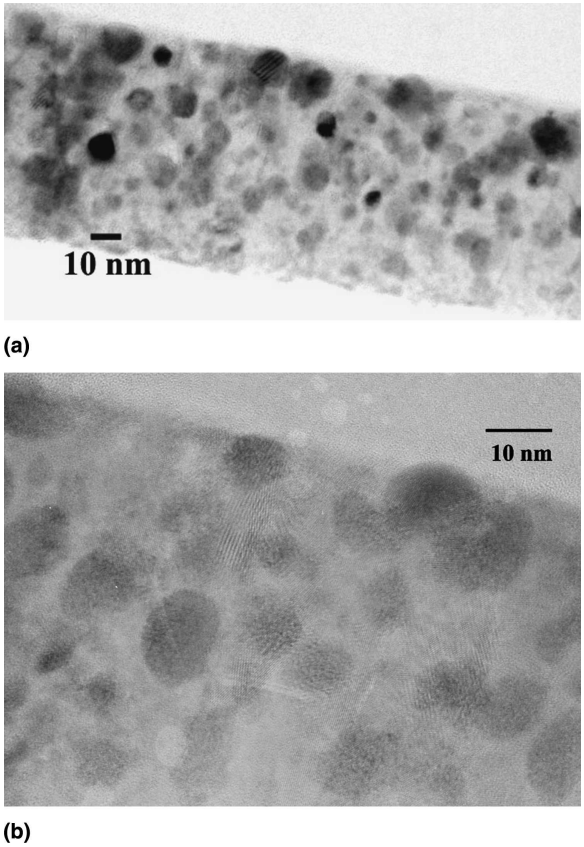

FIG. 3. Typical TEM cross-sectional bright-field image of a Au-YSZ film annealed at 900 °C at (a) low magnification and (b) high magnification.

expected shift in average surface nanoparticle size to larger values is observed with higher annealing temperature, due primarily to the availability of increased thermal energy with higher annealing temperature for further grain coalescence and growth.

Figure 6 plots the results of SEM analyses of the average surface particle size, along with their analogues from XRD analyses of the average Au crystallite size within the YSZ matrix. The SEM and XRD results are in good agreement regarding the size evolution of surface and bulk Au nanoparticles for annealing temperatures below 800 °C. However, as the annealing temperature is driven above 800 °C, the surface nanoparticle size

TABLE I. Summary of pertinent microstructural properties for Au-YSZ nanocomposite films as a function of annealing temperature.

Annealing T (°C))	XRD particle diameter (nm)	SEM particle diameter (nm)	Spectroscopic ellipsometry				
			Standard deviation of fit ($\times 10^{-4}$)	Roughness (nm)	Thickness (nm)	Au vol%	$\gamma(s^{-1})$
600	4.7	7.5	3.7	4.7	95.5	11.2	1.40×10^{15}
700	7.7	8.2	4.0	5.1	90.5	11.4	1.14×10^{15}
800	9.0	11.5	7.6	4.4	81.2	10.5	1.64×10^{14}
900	11.4	16.5	7.7	5.1	86.6	9.7	1.05×10^{14}
1000	14.8	33.8	9.4	12.7	77.7	9.0	9.42×10^{13}

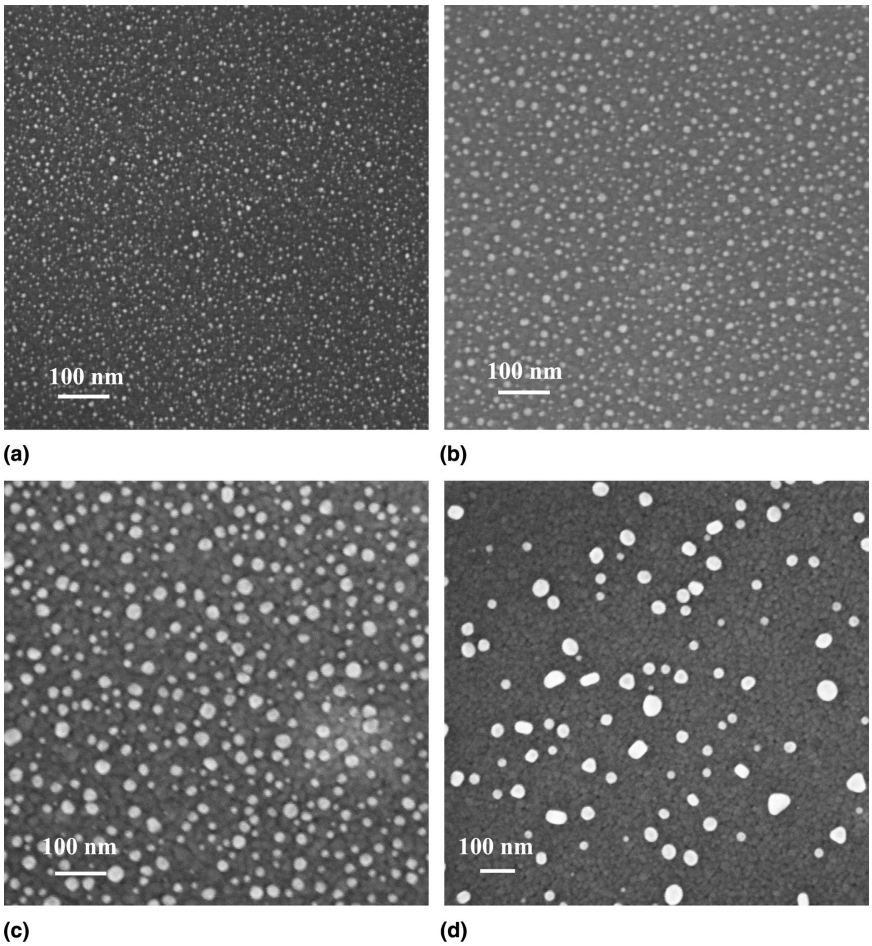

FIG. 4. Typical SEM micrographs of the surface topography of Au-YSZ films: (a) as-deposited, (b) annealed at 700 °C, (c) annealed at 900 °C, and (d) annealed at 1000 °C.

exhibits a significantly larger increase than the crystallite size of bulk nanoparticles. This experimentally observed behavior can be attributed to the enhanced mobility of surface Au atoms in comparison with their embedded counterparts, particularly as a larger thermal energy is made available at the higher annealing temperatures to further activate grain coalescence and growth. This observation is supported by RBS analysis, which revealed the absence of any bulk Au diffusion to the film surface, thus eliminating the possibility of any bulk Au contribution to the increase in Au surface nanoparticle size with temperature.

Figure 7 shows typical SE spectra in the spectral region from 250 to 2000 nm for a sample annealed at 900 °C. The spectra were measured at incident angles of 65°, 70°, and 75°, and fitted as described earlier. Good agreement was achieved between the measured data and the model for all samples as indicated by the standard deviation of the fit. This agreement is documented in Table I, which also lists additional pertinent results from the SE analysis. In particular, it is noted that film thickness, defined as the sum of the layer's surface roughness and actual thickness, is quite invariable for all samples and is in good agreement with the value of ~90 nm obtained from SEM measurements. Similarly, the Au volume fraction is fairly constant for all samples, with a value of ~10 vol%. This result is consistent with the RBS and AES data.

In addition, surface roughness values for films annealed at temperatures below 900 °C are quite consistent ~5 nm. However, a noticeable increase in surface roughness to ~13 nm was observed after annealing at 1000 °C. This increase can be directly correlated to the marked rise in the size of surface Au particles, as documented by the SEM analysis reported in Figs. 4 and 5.

The refractive indexes and extinction coefficients of Au-YSZ nanocomposites are plotted in Fig. 8, along with the measured refractive index of the YSZ matrix ($n \sim 2.1$). As can be seen in Fig. 8(a), film refractive index was found to follow a normal dispersion behavior, except in the immediate wavelength region ~600 nm, where it was observed to increase with increasing wavelength. This behavior is expected, since in this narrow wavelength region, the extinction coefficient reaches a maximum, and thus the experimentally observed anomalous dispersion of the refractive index is consistent with

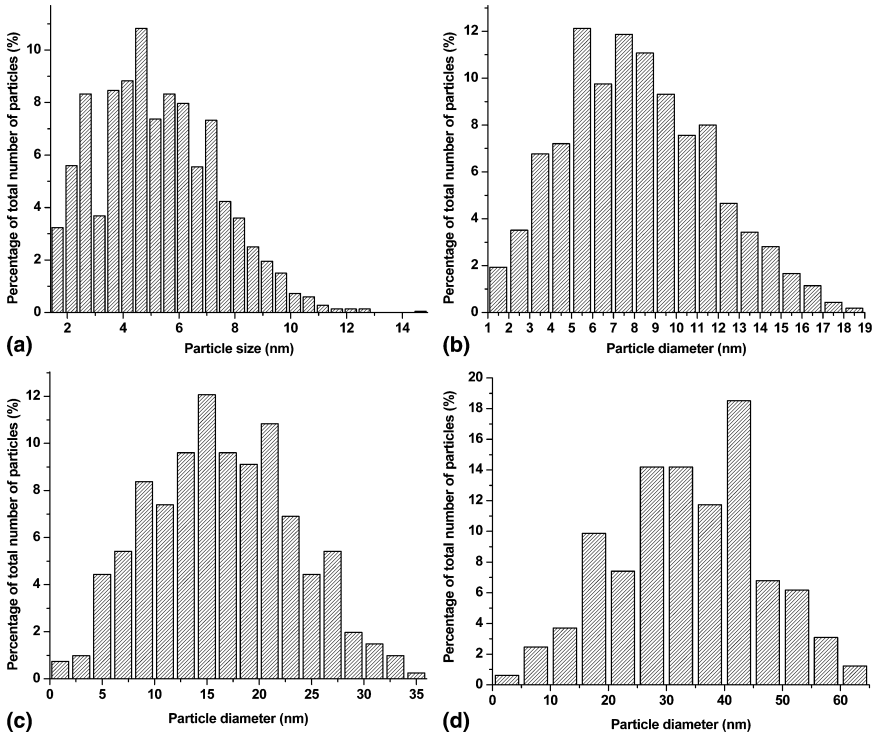

FIG. 5. Corresponding histograms of the surface particle size distribution for Au-YSZ films: (a) as deposited, (b) annealed at 700 °C, (c) annealed at 900 °C, and (d) annealed at 1000 °C.

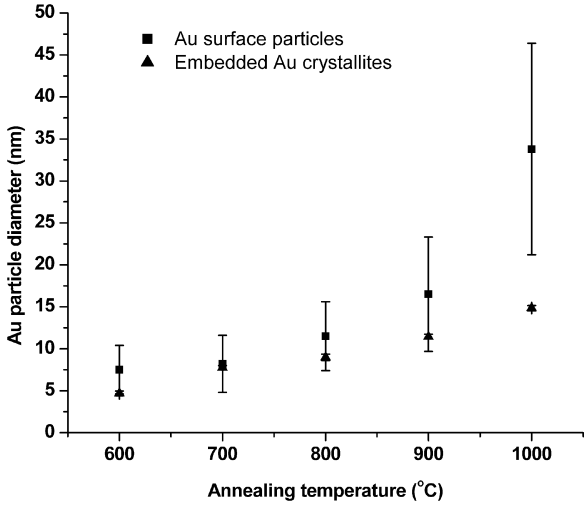

FIG. 6. Average XRD (bulk) and SEM (surface) Au nanoparticle size versus temperature.

the Kramers–Kronig relations.[21] Additionally, at longer wavelengths, the refractive index for all films levels off at ~2.4, indicating that the incorporation of ~10 at.% Au in the YSZ matrix results in an ~14% increase in the refractive index of the nanocomposite as compared to that of the YSZ matrix, despite the fact that bulk Au has a refractive index below 2.0 at this wavelength region. This behavior can be understood within the context of the Lorentz model. Specifically, due to the SPR band of the Au nanoparticles, which is manifested as a peak in the extinction coefficient of the nanocomposites, the overall refractive index obtains higher values than would be intuitively expected by simply mixing the refractive indices of bulk Au and YSZ at longer wavelengths within the measured wavelength range.

Also, as can be seen in Fig. 8(b), the film extinction coefficient reaches a maximum around 600 nm. This maximum is associated with the SPR band of Au nanoparticles. As the annealing temperature and, correspondingly, the average Au nanoparticle size increase, the band red-shifts and becomes narrower and more intense. The dashed vertical line at 595 nm corresponds to the position of the SPR band as predicted from the Mie theory using dielectric functions for bulk Au[22] and for YSZ as measured by spectroscopic ellipsometry. This SPR band behavior is well documented in the literature and indicates that the predictions of the model can be qualitatively understood within the context of the Mie theory and its size-dependent dielectric functions.[6]

Furthermore, Figs. 9(a) and 9(b) display the model derived behavior of, respectively, the real and imaginary parts of the dielectric function for Au nanoparticles. The data for bulk Au, as obtained from Johnson and Christy, is also included for comparison purposes.[22] As observed in Fig. 9(a), the real part of the Au dielectric function (ϵ_{real}) was found to decrease with increasing particle size and behave more like that for bulk Au for annealing temperatures above 800 °C. This behavior is in disagreement with the trend reported by Quinten[23] and

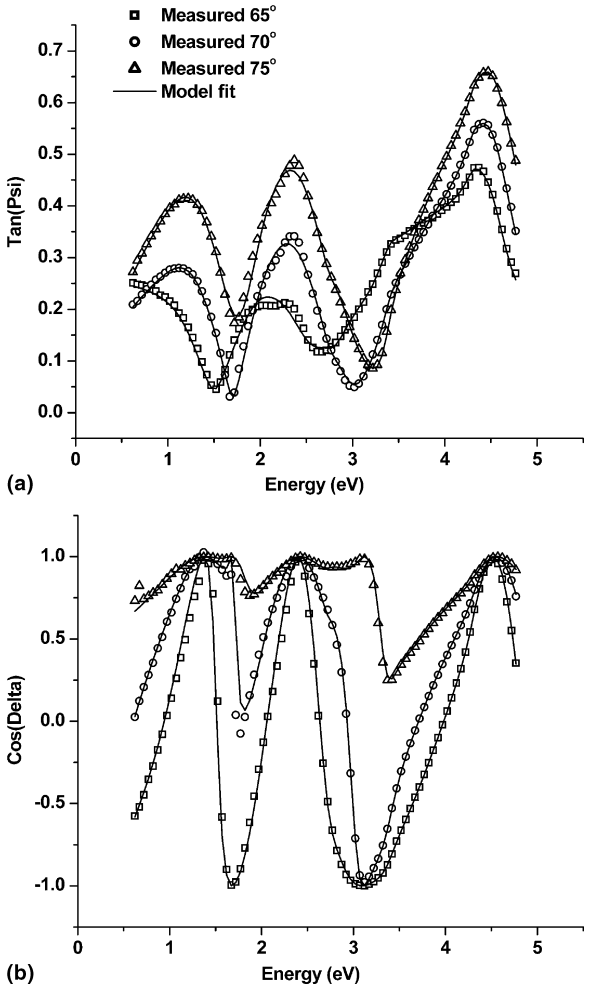

FIG. 7. Ellipsometric data for Au-YSZ nanocomposite film after annealing at 900 °C, as measured at angles of incidence of 65°, 70°, and 75°, and model fits: (a) Tan(Psi), (b) Cos(Delta).

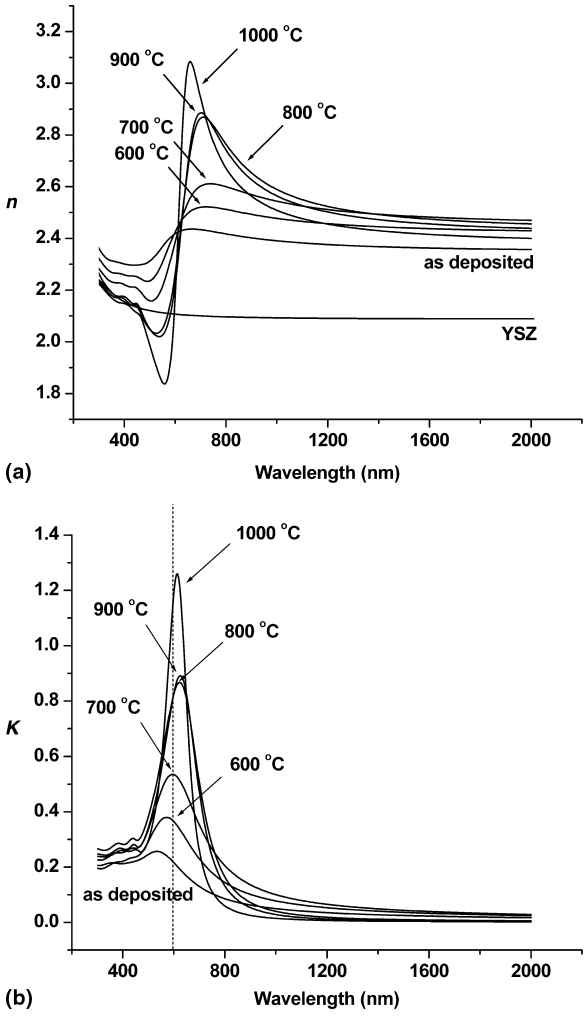

FIG. 8. Optical constants of Au-YSZ nanocomposite films as a function of annealing temperature: (a) refractive index and (b) extinction coefficient. The dashed line indicates the position of the SPR band as predicted from the Mie theory using bulk dielectric functions for Au.

Kriebig[24] from a Kramers–Kronig analysis of absorption spectra, and the trend obtained by Dalacu[25] from a spectroellipsometric analysis of Au-SiO_2 nanocomposite films between 300 and 1000 nm. All three studies reported an increase in ϵ_{real} with increasing Au particle size.

In terms of the imaginary part (ϵ_{imag}) of the Au dielectric function, Fig. 9(b) shows a significant decrease in $\epsilon_{imag.}$ as the annealing temperature increases above 800 °C for wavelengths above 500 nm. In this region, $\epsilon_{imag.}$ is mostly determined by the behavior of free electrons and is thus described by Drude law. This behavior is indicative of a drastic change in the mean free path for scattering of free electrons. In an effort to elucidate this trend, Fig. 10 plots the scattering frequency obtained by the model versus the inverse of Au particle radius as determined by XRD analysis. The dashed line corresponds to a linear regression analysis using experimental data from absorption measurements of similar films on sapphire substrates.[12] It should be noted that the scattering frequency obtained by the model corresponds to the scattering frequency of the embedded particles, since surface particles are treated as a rough interface within the context of the model. While XRD analysis provides the average particle size pertaining to both embedded and surface particles, the concentration of the surface particles is significantly lower than that of the embedded ones. Therefore, we have approximated the embedded particle size as being equal to the XRD-determined average particle size.

As can be seen from the figure, the scattering frequency follows the linear trend obtained from the absorption data for samples annealed above 800 °C. Conversely, for the samples that were annealed below 800 °C, the scattering frequency exhibits a drastic increase. These results clearly show that although the model is successful at qualitatively and quantitatively describing the evolution of Au nanoparticle size as the annealing temperature increases above 800 °C, the size is

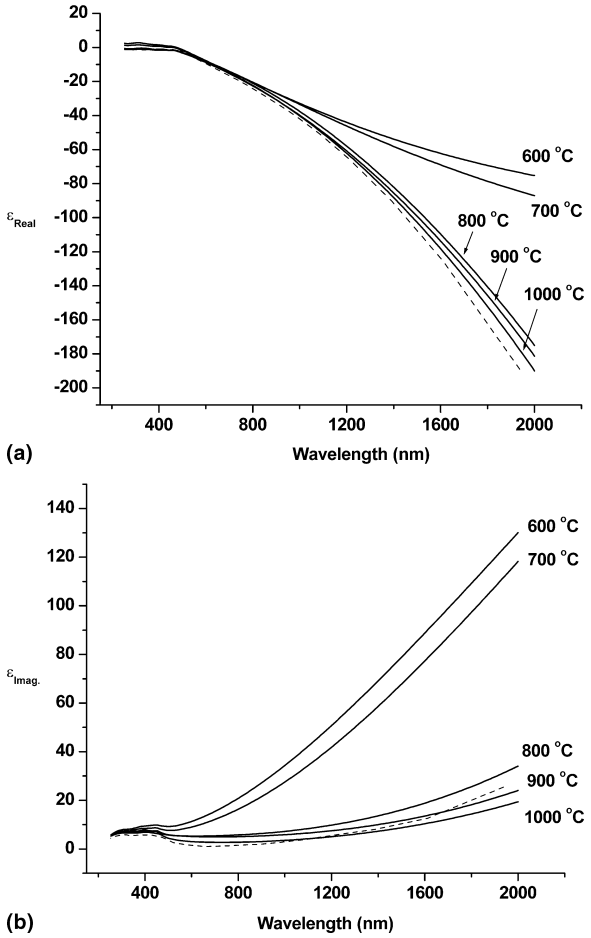

FIG. 9. Optical constants of Au obtained by SE analysis: (a) ϵ_{Real}, (b) ϵ_{Imag}. Data for bulk Au are also plotted as a dashed line for comparison purposes.

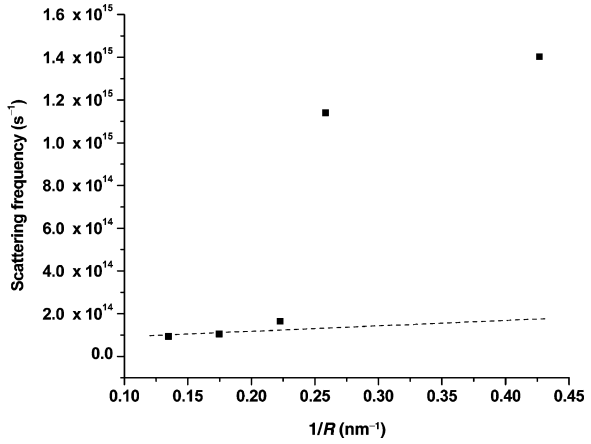

FIG. 10. Scattering frequency of Au as a function of the inverse of the nanoparticle radius. The dashed line corresponds to a linear regression analysis on measured absorption data of similar films.

significantly underestimated for the samples that were annealed below 800 °C with respect to results obtained from standard SPR band analysis.

These discrepancies suggest the existence of other factors that have a significant influence on the optical behavior of the Au-YSZ nanocomposites and thus must be taken into account within the context of the present model. In this respect, the model used for analyzing the ellipsometric data assumes the presence of only Au nanoparticles in the YSZ matrix. However, the results reported herein show that Au also exists in atomic form within the YSZ matrix, and associated contributions are added on to those from Au nanoparticles. As such, the value of the dielectric function deviates significantly from what would be expected for Au nanoparticles of a certain diameter, primarily due to the presence of atomic Au in the nanocomposite. Notably, due to the considerable contribution of atomic Au in the optical behavior of the Au-YSZ nanocomposites, it would have been more accurate to model the Au-YSZ nanocomposites as a three material system consisting of YSZ, Au nanoparticles, and atomic Au. However, this was not possible within the context of the software used for the ellipsometric analysis.

The as-deposited Au-YSZ films are comprised of a mixture of atomic Au and Au nanoclusters with diameter smaller than 2 nm. As the annealing temperature increases, the concentration of Au in nanoparticle form increases at the expense of the concentration of Au in atomic form. This is consistent with the evolution of the microstructure of the films with temperature as discussed above, and accounts for the marked decrease in the real and imaginary parts of the dielectric functions of Au as the annealing temperature is raised above 800 °C. Below this temperature, the model fails to quantitatively describe the progression of Au nanoparticle diameter, due to the considerable contribution from atomic Au. This observation is in good agreement with prior work that showed that the dielectric functions of Au clusters with sizes smaller than 3 nm cannot be described solely within the context of bulk dielectric functions and the reduced mean free path for scattering of free electrons[26] and requires the addition of a wavelength independent offset to obtain good agreement with experimental data.

V. CONCLUSIONS

Au-YSZ nanocomposite films were synthesized using rf magnetron co-sputtering in combination with post-deposition annealing. The optical constants of the resulting films were determined by spectroscopic ellipsometry and modeled within the context of M-G effective medium theory. The extinction coefficient was found to exhibit a maximum at ~600 nm associated with the SPR band of Au nanoparticles. In the same wavelength region, the refractive index was found to follow an anomalous dispersion behavior. However, at longer wavelengths, an increase of ~20% was observed in the refractive index of Au-YSZ nanocomposites with respect to

that of the YSZ matrix. This increase was attributed to the incorporation of Au within the YSZ. The model was successful at predicting the evolution of Au nanoparticle size with increasing annealing temperature above 800 °C. For lower annealing temperatures, the average Au nanoparticle size was significantly underestimated by the model, as compared to standard interpretation of the SPR bands. This behavior was attributed to the relatively high concentration of atomic Au present in the YSZ matrix at the lower annealing temperatures.

ACKNOWLEDGMENTS

This work was supported by the United States Department of Energy National Energy Technology Laboratory under contract number DE-FG26-04NT42184 and the New York State Office of Science, Technology and Academic Research (NYSTAR). This support is gratefully acknowledged.

REFERENCES

1. I. Tanahashi, Y. Manabe, T. Tohda, S. Sasaki, and A. Nakamura: Optical nonlinearities of Au/SiO_2 composite thin films prepared by a sputtering method. *J. Appl. Phys.* **79,** 1244 (1996).
2. H.B. Liao, R.F. Xiao, and G.K.L. Wong: Large third-order nonlinear optical susceptibility of Au-Al_2O_3 composite films near the resonant frequency. *Appl. Phys. B. Lasers Opt.* **65,** 673 (1997).
3. H. Liao, R.F. Xiao, H. Wong, K.S. Wong, and G.K.L. Wong: Large third-order optical nonlinearity in Au:TiO_2 composite films measured on a femtosecond time scale. *Appl. Phys. Lett.* **72,** 1717 (1998).
4. A.D. MacFarland and R.P. Van Duyne: Single silver nanoparticles as real-time optical sensors with zeptomole sensitivity. *Nano Lett.* **3,** 1057 (2003).
5. M. Ando, T. Kobayashi, S. Iijima, and M. Haruta: Optical CO sensitivity of Au–CuO composite film by use of the plasmon absorption change. *Sens. Actuators B* **96,** 589 (2003).
6. U. Kreibig and M. Vollmer: *Optical Properties of Metal Clusters*; Springer: New York, 1995; p. 23.
7. T. Girardeau, S. Camelio, D. Babonneau, J. Toudert, and A. Barranco: Correlations between the microstructure of Ag-Si_3N_4 multilayers and their optical properties. *Thin Solid Films* **455,** 313 (2004).
8. P. Zhou, H. You, J. Jia, J. Li, T. Han, S. Wang, R. Zhang, Y. Zheng, and L. Chen: Concentration and size dependence of optical properties of Ag:Bi_2O_3 composite films by using the co-sputtering method. *Thin Solid Films* **455,** 605 (2004).
9. R. Roy, S. Mandal, D. Bhattacharyya, and A.K. Pal: An ellipsometric investigation of Ag/SiO_2 nanocomposite thin films. *Eur. Phys. J. B* **34,** 25 (2003).
10. J.C.G. de Sande, R. Serna, J. Gonzalo, C.N. Alfonso, D.E. Hole, and A. Naudon: Refractive index of Ag nanocrystals composite films in the neighborhood of the surface plasmon resonance. *J. App. Phys.* **91,** 1536 (2002).
11. S. Cho, H. Lim, K.S. Lee, T.S. Lee, B. Sheong, W.M. Kim, and S. Lee: Spectro-ellipsometric studies of Au/SiO_2 nanocomposite films. *Thin Solid Films* **475,** 133 (2005).
12. G. Sirinakis, R. Siddique, C. Monokroussos, M.A. Carpenter, and A.E. Kaloyeros: Microstructure and optical properties of Y_2O_3-stabilized ZrO_2-Au nanocomposite films. *J. Mater. Res.* **20,** 2516 (2005).
13. B.D. Cullity and S.R. Stock: *Elements of X-ray Diffraction,* 3rd ed. (Prentice-Hall, Upper Saddle River, NJ, 2001).
14. A.R.L. Thermo: A Lorentzian peak is more appropriate than a Gaussian profile when the broadening of the XRD peak is due to nanograins instead of stress or strain. (private communication).
15. J.C. Maxwell Garnett: Colours in metal glasses and in metallic films. *Philos. Trans. R. Soc.* **A203,** 385 (1904).
16. Pierre Boher: SOPRA WinElli version 4.07 (1994).
17. H. Hövel, S. Fritz, A. Hilger, U. Kreibig, and M. Vollmer: Width of cluster plasmon resonances: Bulk dielectric functions and chemical interface damping. *Phys. Rev. B* **48,** 18178 (1993).
18. N.W. Ashcroft and N.D. Mermin: *Solid State Physics*, (Saunders College Publishing, Philadelphia, PA, 1976).
19. B.N.J. Persson: Polarizability of small spherical metal particles: Influence of the matrix environment. *Surf. Sci.* **281,** 153 (1993).
20. G. De Marchi, G. Mattei, P. Mazzoldi, C. Sada, and A. Miotello: Two stages in the kinetics of gold cluster growth in ion-implanted silica during isothermal annealing in oxidizing atmosphere. *J. Appl. Phys.* **92,** 4249 (2002).
21. C.F. Bohren and D.R. Huffman: *Absorption and Scattering of Light by Small Particles*, (Wiley, New York, 1983).
22. P.B. Johnson and R.W. Christy: Optical constants of the noble metals. *Phys. Rev. B* **6,** 4370 (1972).
23. M. Quinten: Optical constants of gold and silver clusters in the spectral range between 1.5 eV and 4.5 eV. *Z. Phys. B* **100,** 211 (1996).
24. U. Kriebig: In *Growth and Properties of Metal Clusters,* edited by J. Bourdon (Elsevier Scientific, Amsterdam, The Netherlands, 1980), p. 371.
25. D. Dalacu and L. Martinu: Spectroellipsometric characterization of plasma-deposited Au/SiO_2 nanocomposite films. *J. Appl. Phys.* **87,** 228 (2000).
26. M.M. Alvarez, J.T. Khoury, T.G. Schaaff, M.N. Shafigullin, I. Vezmar, and R.L. Whetten: Optical absorption spectra of nanocrystal gold molecules. *J. Phys. Chem. B* **101,** 3706 (1997).